# Radiation beaming in the quantum regime

T. G. Blackburn [1,*] D. Seipt,[2] S. S. Bulanov,[3] and M. Marklund[1]
[1]*Department of Physics, University of Gothenburg, SE-41296 Gothenburg, Sweden*
[2]*Center for Ultrafast Optical Science, University of Michigan, Ann Arbor, Michigan 48109, USA*
[3]*Lawrence Berkeley National Laboratory, Berkeley, California 94720, USA*

(Received 30 April 2019; revised manuscript received 6 December 2019; published 10 January 2020)

Classical theories of radiation reaction predict that the electron motion is confined to the plane defined by the electron's instantaneous momentum and the force exerted by the external electromagnetic field. However, in the quantum radiation reaction regime, where the recoil exerted by individual quanta becomes significant, the electron can scatter "out of plane," as the photon is emitted into a cone with finite opening angle. We show that Monte Carlo implementation of an angularly resolved emission rate leads to substantially improved agreement with exact QED calculations of nonlinear Compton scattering. Furthermore, we show that the transverse recoil caused by this finite beaming, while negligible in many high-intensity scenarios, can be identified in the increase in divergence, in the plane perpendicular to the laser polarization and wave vector, of a high-energy electron beam that interacts with a linearly polarized, ultraintense laser.

DOI: 10.1103/PhysRevA.101.012505

## I. INTRODUCTION

Recent advances in the development of high-intensity lasers [1–3] and plasma-based accelerators [4–6] have made it possible to perform experiments on the interaction of charged particles with ultraintense electromagnetic pulses in regimes previously unexplored [7,8]. Earlier experiments relied on conventional accelerator technology [9,10]. The processes studied belong to the field of high-intensity particle physics [11–13], which combines quantum electrodynamics (QED) with the theory of strong electromagnetic (EM) background fields [14]. Of particular significance is photon emission, because the recoil it exerts can dominate the dynamics of electrons and positrons in high-field environments, including neutron-star magnetospheres [15] and laser-matter [16–18] or laser-laser [19–22] interactions in next-generation facilities [23–25].

Here we revisit how this fundamental process is modeled in simulations of particle dynamics in strong EM fields. In contrast to previous work, we employ a photon emission rate that is differential in scattering angle as well as energy, thereby resolving the beaming of the radiation around the emitting particle's instantaneous velocity. As a result, the accuracy of simulations based on Monte Carlo implementation of localized emission events [26,27] is substantially improved, when benchmarked against exact QED predictions of nonlinear Compton scattering [28]. Simulations in the multiphoton, quantum radiation reaction regime demonstrate that including the beaming is important for accurate modeling of the emission of moderate-energy photons. The consequent transverse recoil may be neglected in many high-intensity scenarios, but is distinguishable in the increase in the divergence of an electron beam that collides with a linearly polarized laser pulse, for experimental parameters accessible with present-day technology. Furthermore, employing an angularly resolved spectrum permits quantitative estimation of the accuracy of the simulations in the low-energy part of the photon spectrum, where interference, i.e., nonlocal, effects become important.

In natural units $\hbar = c = 1$ (as used throughout), the photon emission rate per unit of proper time, energy $\omega'$, and polar and azimuthal scattering angles $\theta$ and $\varphi$ is [29]

$$W^{(3)} = \frac{\partial^3 W}{\partial u \partial z \partial \varphi} = \frac{\alpha m}{3\sqrt{3}\pi^2 \chi} \frac{u}{(1+u)^3} \times \{z^{2/3}[1+(1+u)^2] - (1+u)\} K_{1/3}\left(\frac{2uz}{3\chi}\right), \quad (1)$$

where $\alpha = e^2/(4\pi)$ is the fine-structure constant, $e$ is the elementary charge, $m$ is the electron mass, $u = \omega'/(\gamma m - \omega')$, $z = [2\gamma^2(1-\beta\cos\theta)]^{3/2}$, and $K$ is a modified Bessel function of the second kind. The spectrum is controlled by the electron's Lorentz factor $\gamma$ (velocity $\beta$) and quantum nonlinearity parameter $\chi = e|F_{\mu\nu}p^\nu|/m^3$. Here $F$ is the EM field tensor and $p$ is the electron momentum. The parameter $\chi$ may be interpreted as the ratio of the rest-frame electric-field strength to that of the critical field of QED $E_{\mathrm{cr}} = m^2/e$ [30,31], or as the magnitude of the proper acceleration in natural units.

The radiation is strongly beamed around the particle's instantaneous velocity if the particle is ultrarelativistic [14,32]. The mean-square angle of the power spectrum, $\langle\theta^2\rangle = \int \theta^2 \omega' W^{(3)} du dz d\varphi / \int \omega' W^{(3)} du dz d\varphi$, is $\langle\theta^2\rangle \simeq 5/(4\gamma^2) \ll 1$ in the classical limit $\chi \ll 1$. It is larger in the quantum regime, growing as $\langle\theta^2\rangle \simeq 1.76\gamma^{-2}\chi^{2/3}$ for $\chi \gg 1$, but still small. This justifies the standard approximation used in simulation codes that photons are emitted parallel to the particle momentum [26,27]. Nevertheless, its inclusion is warranted because the degree of beaming depends on the photon

*tom.blackburn@physics.gu.se

 

energy as well as the electron energy. The mean-square angle at fixed photon energy $\omega' = \gamma m u/(1+u)$, $\langle\theta^2(\omega')\rangle = \int \theta^2 W^{(3)} dz d\varphi / \int W^{(3)} dz d\varphi$, is, to leading order in $\chi/u$,

$$\gamma^2\langle\theta^2(\omega')\rangle = \begin{cases} \frac{\Gamma(4/3)}{\Gamma(2/3)}(3\chi/u)^{2/3}, & \chi/u \gg 1 \\ \chi/u, & \chi/u \ll 1 \end{cases}. \tag{2}$$

The lower the photon energy, the larger its emission angle: note that, for $\omega' \ll \gamma m$, $u \simeq \omega'/(\gamma m)$.

We have implemented a Monte Carlo algorithm that samples the triple-differential spectrum into a particle-tracking code, as an alternative to the standard method in which only the energy is sampled from the angularly integrated spectrum. These discrete emission events occur stochastically along the particles' classical trajectories; between them, the dynamics are determined by the Lorentz force alone. The electron recoil on emission is fixed by the conservation of momentum. This "semiclassical" approach to QED is appropriate if the normalized amplitude of the field $a_0$ satisfies $a_0^3/\chi \gg 1$, such that the formation lengths of the photons are much smaller than the timescale of the external field [14,33] and emission rates for a "locally constant" field can be employed.

We first confirm this by comparing the results of simulations which include the radiation beaming, with exact QED in Sec. II. We propose a conceptually simple way to estimate the magnitude of the error made by the locally constant field emission rate used in simulations. Then in Secs. III and IV we predict the beaming's effect on the radiation spectrum and electron dynamics in experimentally relevant scenarios, where multiple photon emissions and the spatiotemporal structure of the focusing laser field are taken into account.

## II. IMPROVED AGREEMENT WITH EXACT QED

Sampling the angularly resolved emission spectrum leads to substantially improved agreement with exact QED results. The interaction we consider is single nonlinear Compton scattering, i.e., the emission of one and only one photon by an electron in an intense, pulsed plane EM wave. The field tensor for the pulse is $eF_{\mu\nu} = m a_0 \sum_i k_{[\mu}\varepsilon^i_{\nu]}\frac{d\psi_i}{d\phi}$, where $(\psi_1, \psi_2) = (\cos\phi, \delta\sin\phi)\cos^2[\phi/(4\sigma)]$ for $|\phi| \leqslant 2\pi\sigma$, $\phi$ is the phase, $\delta = 1$ and 0 for circular and linear polarization, $k$ is the wave vector, and $\varepsilon_{1,2}$ are the polarization vectors along $x$ and $y$, respectively.

The one-photon emission probability is calculated in the framework of strong-field QED, which accounts for the interaction with the background electromagnetic field to all orders in $a_0$ [34–36]. The total probability, which can exceed unity, is interpreted as the mean number of emissions $N_\gamma$ [14,37]. As our Monte Carlo simulations allow for the emission of an arbitrary number of photons, equivalent results are obtained by postselection [28]: photon spectra are generated statistically using only those simulated collisions in which exactly one photon is emitted, and then rescaled to have the integral equal to the mean number of emissions, as determined from the full set of collisions.

A comparison between exact QED results and simulations that do and do not include the finite beaming of the radiation is presented in Fig. 1. Results are given in terms of the emitted photon's normalized perpendicular momenta $mr_{x,y} = k'_{x,y}(kp_0/kk')$, where $p_0$ is the initial electron momentum. The $r_x$-$r_y$ spectrum is effectively the angular profile of the emitted radiation if $\gamma_0 \gg a_0 \gg 1$, as $r_{x,y} \simeq \gamma_0\theta_{x,y}$ for $\tan\theta_{x,y} = k'_{x,y}/(-k'_z)$. We consider two examples: an electron with $\gamma_0 = 3000$ collides with a circularly polarized pulse with $a_0 = 20$, and an electron with $\gamma_0 = 1 \times 10^4$ collides with a linearly polarized pulse with $a_0 = 25$. $\sigma = 3$ and the central frequency $\omega = k^0 = 1.55$ eV in both cases.

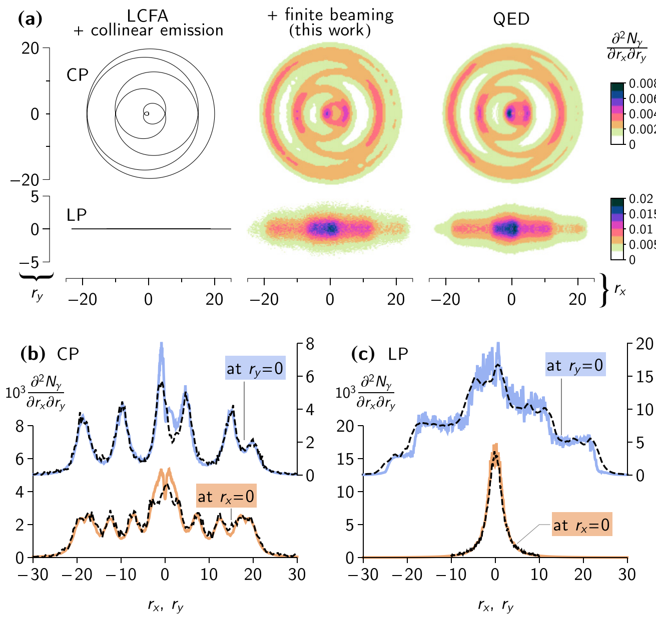


FIG. 1. Agreement with exact QED is improved when simulations using localized emission rates include the finite beaming of the radiation. (a) Differential probability that an electron emits a single photon with normalized perpendicular momenta $r_{x,y}$ in a circularly polarized (CP) or linearly polarized (LP) EM wave. (b, c) Lineouts along $r_{x,y} = 0$: results from QED (solid colors) and simulations that include finite beaming (black, dashed).

If the finite beaming is neglected, the calculated photon spectrum collapses onto a curve that traces the electron trajectory: $mr_{x,y} = p_{x,y}(\phi)$. This causes the angular spread of the radiation to be significantly underestimated [28]. By contrast, when the finite beaming is included [central column of Fig. 1(a)], we obtain excellent agreement with the QED results [right column of Fig. 1(a)]. The structure of the angular profile is reproduced in both the circularly and linearly polarized cases, as is shown by the lineouts along the axes $r_x = 0$ and $r_y = 0$ in Figs. 1(b) and 1(c).

Models based on localized emission, as ours is, are accurate for photons with energies $\omega'/(\gamma m) \gtrsim \chi/a_0^3$. Low-energy photons, or those that are emitted in low-intensity regions of the pulse, have long formation lengths and interference effects tend to suppress their emission [38]. Hence we observe discrepancies near $r_x = r_y = 0$ in the circularly polarized case, because photons in this region originate from the pulse head and tail where the local value of $a_0 \not\gg 1$. Similarly, the spectrum in the linearly polarized case is broader in the $r_x$ direction near the turning points $\partial_\phi r_x = 0$, where the local field vanishes.

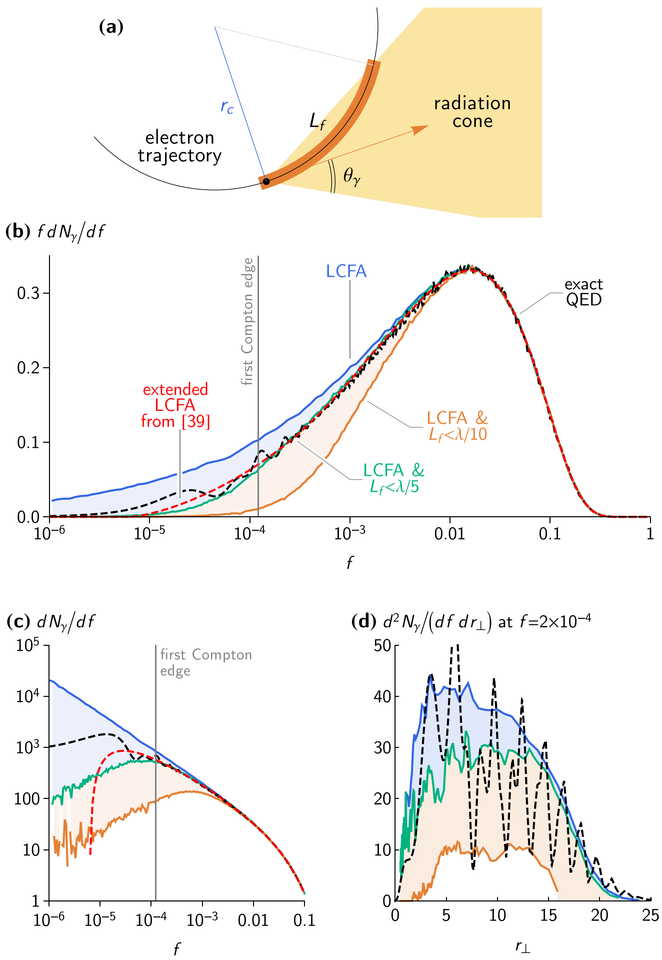


FIG. 2. Estimating the error made in neglecting the finite formation length of the emitted photon, at $a_0 = 10$: (a) the relation between the formation length and the angle at which the photon is emitted; (b, c, d) comparison of results from exact QED (black, dashed) and simulations where only photons with formation lengths $L_f < \lambda/10$ (orange), $\lambda/5$ (green), or infinity (blue) are emitted. In (b, c) we also show the result using the "extended" LCFA rates presented in [39] (red, dashed). In (d) we have chosen a value of $r_\perp$ that lies in the region where the validity of the LCFA is questionable.

The finite formation length of the photon is a significant potential source of error in simulations based on localized emission rates [28]. If this length is comparable to the spatial scale of variation of the background field, nonlocal effects such as quantum interference become important. We now discuss how sampling the angularly resolved photon spectrum allows the magnitude of such effects to be estimated. Observe that, in the classical picture, the formation length of a photon emitted at angle $\theta$ to the electron instantaneous momentum is the distance traveled by the electron before it has separated from the photon by at least $\theta$ [see Fig. 2(a)]. This distance may be estimated locally as $L_f \simeq 2r_c\theta$, where the instantaneous radius of curvature of the electron trajectory

$$r_c = \frac{\gamma^2 - 1}{\sqrt{m^2\chi^2 - m^2(\vec{E} + \vec{v} \times \vec{B})^2/E_{\text{cr}}^2}} \tag{3}$$

can be calculated using the Frenet-Serret formalism, assuming that only electromagnetic forces are acting on the electron [40]. For all practical purposes, the curvature radius can be approximated as $r_c \simeq \gamma^2/(m\chi)$, as is done in this paper. $L_f$ can then be calculated for each simulated photon on emission, using the sampled value of the angle $\theta$, and if it exceeds a specified maximum value the photon is not emitted.

Note that, because photons are only ever removed, this procedure does not account for constructive interference effects that could enhance photon emission. However, as it has been shown that the locally constant field approximation (LCFA) tends to lead to overestimation of the low-energy part of the spectrum [28,38,41], comparing the results from simulations with and without this formation length check provides a conceptually simple way to estimate the accuracy of the spectra predicted.

An example of this procedure is shown in Fig. 2, which gives spectra that are differential in $f = kk'/kp_0$, the lightfront-momentum transfer fraction, and $r_\perp = (r_x^2 + r_y^2)^{1/2}$, for the photon emitted in the collision of the electron with $\gamma_0 = 1000$ and a circularly polarized laser pulse with $a_0 = 10$ and $\sigma = 3$. All three simulations include the finite beaming of the radiation, but take different values of the maximum permitted formation length. Observe that the spectra without a maximum (blue lines) and $L_f < \lambda/10$ (orange lines) bracket the exact QED result; the difference between the two illustrates the expected accuracy of the LCFA.

Figure 2(d) shows the double-differential spectrum at constant $f = 2 \times 10^{-4}$, which lies in the region $f \lesssim 2\chi/a_0^3$, where this accuracy is weakest. The estimated error is large, warning that substantial interference effects are expected, as visible in the exact QED result. In fact, the best agreement is obtained with a formation length cutoff of $\lambda/5$ (green lines in Fig. 2), which lies in between the two extreme cases. It is similar to the result of a simulation using the "extended" photon emission rates derived by Ilderton *et al.* [39]. As this approach is based on gradient corrections to the LCFA, two filters are necessary: one for the correction, which is activated only for $a(\phi) > c = \pi/2$, and a global filter ensuring positivity of the rate. Note that the extended rates are presented only in their angularly integrated form and thus we cannot compare the angularly resolved spectra shown in Fig. 2(d). We could obtain one by assuming collinear emission, but it would have a hard cutoff at $r_\perp = a_0 = 10$, which is not consistent with exact QED [28].

The procedure we have outlined uses only *local* quantities $(\chi, \gamma)$ to estimate the formation length and it is therefore independent of the specific structure of the background field. However, if we explicitly choose this to be an EM wave, where $\chi = 2a_0\gamma\omega/m$, and take $\theta \simeq 1/\gamma$ as representative of the whole photon spectrum, we recover the well-known result that $L_f \simeq 1/(a_0\omega)$ [14]. On the other hand, using Eq. (2) indicates how the formation length depends on the photon energy $\omega'$:

$$L_f \simeq \frac{\chi^{1/3}}{a_0\omega}\left(\frac{\gamma m - \omega'}{\omega'}\right)^{1/3}. \tag{4}$$

This is consistent with the results of Di Piazza *et al.* [41]. No matter how large $a_0$ is, photons with sufficiently low energy can have formation lengths comparable to the laser wavelength. Our approach optionally excludes such photons on physical grounds, putting error bars on theoretical predictions. This is complementary to the use of corrected LCFA rates [39,41–43], which aim to reduce the error rather than estimate its magnitude.

Thus far we have considered only the emission of a single photon, as this can be calculated within QED and so benchmarking of the angularly resolved LCFA rate Eq. (1) is possible. We now turn to the effect of the radiation beaming on the photon and electron spectra in more realistic scenarios, where we allow for multiple photon emission and spatiotemporal structure in both the laser pulse and electron beam.

## III. BROADENING OF THE RADIATION ANGULAR PROFILE

In a head-on collision with an EM wave that is linearly polarized along $x$, neglect of the finite emission angle means that all photons have $r_y = 0$, confining the radiation emitted by an initially divergence-free electron beam to the laser polarization plane. In reality, photons are emitted with $r_y \neq 0$. Thus, as the initial divergence of the electron beam is reduced to zero, the photon divergence in the perpendicular direction (along $y$) saturates at a nonzero value.

This floor on the final divergence can be estimated analytically in the limit $\chi \ll 1$, where the mean-square polar angle of the instantaneous power spectrum is $\langle\theta^2\rangle = 5/(4\gamma^2)$. The total variance of the radiation angular profile in the $y$ direction, $\delta_\gamma^2$, after the electron has passed through a pulsed plane wave, is obtained by integrating $\frac{1}{2}\langle\theta^2\rangle$ over the pulse temporal profile. Thus we have $\delta_\gamma^2 = \int \frac{1}{2}\langle\theta^2\rangle \mathcal{P}\, d\phi / \int \mathcal{P}\, d\phi$, where $\mathcal{P} = \alpha m^2\chi^2/(3\omega) \propto [\gamma(\phi)g(\phi)]^2$ gives the instantaneous radiated power (per unit phase), $g(\phi)$ is the pulse temporal envelope, and $\gamma(\phi)$ is the electron Lorentz factor as a function of phase $\phi$. We obtain the latter by solution of the Landau-Lifshitz equation [44], which accounts for the deceleration due to classical radiation reaction. Assuming that $g(\phi)$ is slowly varying, this gives $\gamma(\phi) \simeq \gamma_0/[1 + 2\alpha a_0^2\gamma_0\omega\mathcal{I}(\phi)/(3m)]$, where $\mathcal{I}(\phi) = \int_{-\infty}^{\phi} g^2(\psi)\, d\psi$. Therefore

$$\delta_\gamma^2 = \delta_0^2 + \frac{5(1+\mathcal{R})}{8\gamma_0^2}, \quad \mathcal{R} = \frac{2\alpha a_0^2\gamma_0\omega}{3m}\int_{-\infty}^{\infty} g^2(\phi)\, d\phi, \quad (5)$$

where $\delta_0$ is the initial divergence of the electron beam. If the intensity profile $g^2(\phi)$ is a Gaussian with full width at half maximum (FWHM) duration $\tau$, $\int_{-\infty}^{\infty} g^2(\phi)\, d\phi = \omega\tau\sqrt{\pi/(4\ln 2)}$.

We compare this prediction to the results of three-dimensional (3D) simulations of laser-electron collisions. In contrast to our comparison with exact QED in Sec. II, these simulations account for *multiphoton* radiation-reaction effects as well as the spatiotemporal structure of the electron beam and focused laser pulse. The former is initialized with mean energy 500 MeV and root-mean-square (rms) energy spread 50 MeV, divergence $\delta_0 = 0.5$ mrad, and size $\rho = 10\,\mu$m. This corresponds to a normalized transverse emittance of $\epsilon_\perp = [\langle y^2\rangle\langle p_y^2/m^2\rangle]^{1/2} = 5.0$ mm mrad. Much smaller emittances have already been measured in laser-wakefield accelerators [45,46]. The laser pulse has wavelength $\lambda = 0.8\,\mu$m, has duration 30 fs, is linearly polarized along $x$, and is

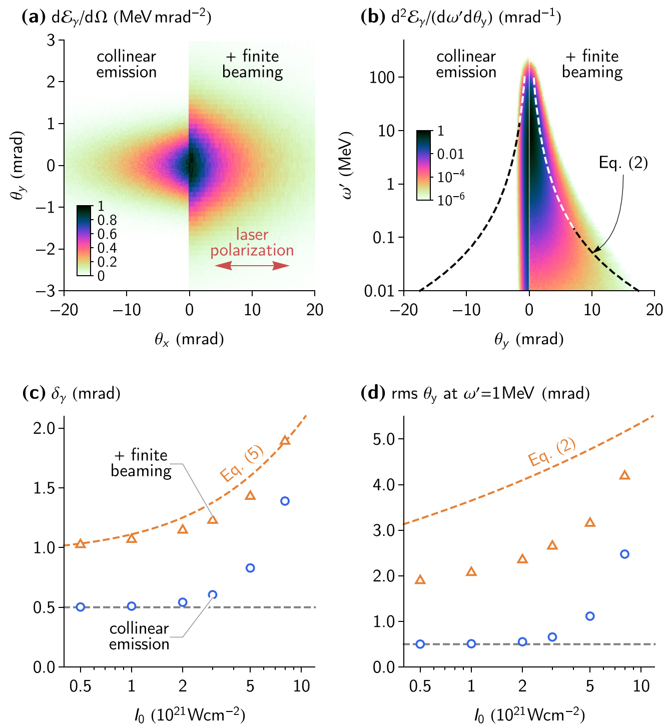


FIG. 3. Effect of the radiation beaming on the angularly resolved photon spectrum, in the collision of a 500-MeV electron beam and a linearly polarized laser pulse with peak intensity $I_0$. Density maps (color scale, normalized to respective maxima) of (a) the energy radiated per unit solid angle and (b) the energy radiated per unit frequency and angle, both at $I_0 = 2 \times 10^{21}$ W cm$^{-2}$. The divergence in the $y$ direction (c) of the total spectrum and (d) at fixed frequency $\omega' = 1$ MeV: simulation results (points), theoretical predictions of Eqs. (2) and (5) (orange, dashed), and the initial beam divergence (gray, dashed).

focused to a spot of size $w_0 = 2.5\,\mu$m and peak intensity $2 \times 10^{21}$ W cm$^{-2}$. The fields in our simulations are calculated to fourth order in the diffraction angle [47].

The photon spectra for this scenario, resolved in $\theta_x$ (the angle in the plane of polarization) and $\theta_y$ (the perpendicular angle), are shown in Figs. 3(a) and 3(b); they are clearly broader in $\theta_y$ when the beaming of the radiation is included. This demonstrates that the increase shown in the upper panel of Fig. 1 can survive more realistic interaction parameters. Furthermore, Fig. 3(b) shows that the angular spread increases as the photon energy is lowered, whereas the entirety of the radiation is confined to $\theta_y \lesssim 3\delta_0$ if emission is assumed to be collinear.

Figures 3(c) and 3(d) give the energy-weighted rms $\theta_y$ of all photons, and only those photons with $\omega' = 1$ MeV, as a function of peak intensity, with all other parameters fixed. Both are in reasonable agreement with our theoretical predictions Eqs. (2) and (5), setting $\chi = 2\gamma_0 a_0\omega/m$ and $\gamma = \gamma_0$ in the former. Note that it is possible for $\delta_\gamma > \delta_0$ even if emission is assumed to be collinear, because the decelerated electrons are ponderomotively expelled from the focal spot in both the $x$ and $y$ directions. In principle, the radiation beaming is also evident in the plane of polarization. However,

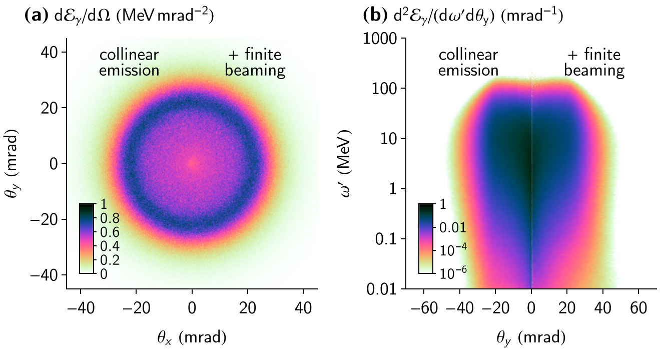


FIG. 4. The effect of the radiation beaming on the angularly resolved photon spectrum is much weaker when the laser is circularly polarized: density maps (color scale, normalized to respective maxima) of (a) the energy radiated per unit solid angle and (b) the energy radiated per unit frequency and angle in the collision of a 500-MeV electron beam and a circularly polarized laser pulse with peak intensity $2 \times 10^{21}$ W cm$^{-2}$.

if $a_0 \gg 1$, the angular extent of the radiation in this direction is dominated by the $a_0/\gamma$ contribution of the electron's oscillation.

The range of photon energies where inclusion of the beaming is essential can be estimated as the range for which the typical emission angle is between two and ten times the global average of $\approx 1/\gamma$. Using our earlier result, Eq. (2), this is $\chi/870 \lesssim u \lesssim \chi/7$, where $\omega'/(\gamma m) = u/(1+u)$. For the parameters used in Fig. 3, this corresponds to photons with energies from 0.1 to a few MeV. Even though they individually contribute little to the total-energy loss, such photons are emitted in far greater numbers than their higher-energy counterparts. As discussed in Sec. II, simulations based on the LCFA tend to overestimate the yield of low-energy photons; thus we validate the results shown in Fig. 3 against simulations in which photons with formation length $L_f > \lambda/10$ are discarded. This reduces the number of 1-MeV photons by 40%, but the additional broadening at this energy due to the finite beaming [Fig. 3(b)] and the total energy radiated per unit solid angle [Fig. 3(a)] are unchanged. Similarly, the angular widths given in Figs. 3(b) and 3(d) are unchanged to within 5%.

It is important to note that, if the laser is circularly rather than linearly polarized, there is no distinction between the two directions perpendicular to the wave vector. The electrons oscillate in $x$ and $y$ and therefore the radiation has a finite angular spread in both directions, even if the initial electron divergence is reduced to zero and the finite beaming is neglected. This is shown in Fig. 4, where we compare the energy emitted per unit solid angle by a 500-MeV electron beam colliding with a circularly polarized, plane-wave, laser pulse, with peak intensity $2 \times 10^{21}$ W cm$^{-2}$, wavelength 0.8 $\mu$m, and duration 30 fs. (The electron beam has rms energy spread 50 MeV and divergence $\delta_0 = 0.5$ mrad.) Comparing Fig. 4 to Fig. 3, it is clear that a distinction between the two perpendicular directions is necessary to observe finite beaming effects. We focus, therefore, on the case of linear polarization.

## IV. QUANTUM LIMIT ON THE ELECTRON-BEAM DIVERGENCE

We now turn to the consequences of noncollinear emission for the electron. The conservation of momentum requires that if the photon is emitted at some finite angle a recoil $\Delta p$ is exerted on the emitting particle in the direction perpendicular to its velocity. $\Delta p = \omega' \sin\theta \simeq mu\sqrt{z^{2/3}-1}/(1+u)$ to leading order in $1/\gamma$; its mean value is $\langle \Delta p \rangle/m \simeq 3\sqrt{3}\pi\chi/40$ for $\chi \ll 1$ and $0.264\chi^{1/3}$ for $\chi \gg 1$. For the perpendicular component of the recoil to have a significant impact on the dynamics, it should be comparable in size to the electron's transverse momentum $p_x = ma_0$. However, $\langle \Delta p \rangle / p_x \simeq 0.4\chi/a_0$ or $0.3\chi^{1/3}/a_0 \ll 1$ in almost all high-intensity scenarios of interest. As such, it is safe to neglect the transverse recoil in models of quantum radiation reaction, even though the emission probability vanishes for $\theta \to 0$ and therefore the recoil is never antiparallel to the instantaneous velocity.

Nevertheless, the effect of this transverse recoil can be visible in the collision of an ultralow emittance electron beam with a high-intensity, *linearly* polarized laser pulse. This is because, in a plane wave, the momentum in the direction perpendicular to the polarization $p_y$ is preserved by the Lorentz force; under classical radiation reaction, it can only ever decrease. Concretely, the equations of motion for this scenario are $\frac{d}{d\phi}(kp) = -2\alpha m^2 \chi^2/3$ and $\frac{d}{d\phi}[p_y/(kp)] = 0$ [44]. We have $p_y = p_{y,0}(kp/kp_0) \leqslant p_{y,0}$ by $\frac{d}{d\phi}(kp) \leqslant 0$, where the equality applies in the absence of radiation reaction. If $p_y = 0$ initially, it remains so. This is no longer the case when the transverse recoil is included.

Provided that radiation losses are not too large, the electron emerges from the laser field with $kp \simeq 2\omega|p_z|$. Therefore the distribution of $\tan\theta_y = p_y/|p_z| \simeq 2\omega(p_y/kp)$ is unchanged under classical radiation reaction. It is unchanged under quantum radiation reaction only if collinear emission is assumed. Including the finite emission angle and associated transverse recoil, by contrast, leads to an increase in the out-of-plane divergence. As the initial divergence of the electron beam is reduced to zero, the final divergence $\delta_e = \langle \theta_y^2 \rangle^{1/2}$ saturates at a nonzero value.

This lower bound on the divergence is a pure quantum effect, arising from the finite number of emissions. This phenomenon will occur not only in an ultraintense laser, as considered here, but also in a static magnetic field. In principle, the transverse recoil sets a lower bound on the emittance of an electron beam in a storage ring, in the direction parallel to the magnetic field [48]; however, this limit is typically four orders of magnitude smaller than the emittance in the plane of the orbit, and in practice is dominated by magnet alignment errors and other deviations.

To estimate the final divergence, we assume that the electron performs a random walk in $\theta_y$, so $\delta_e^2 = \int \frac{1}{2}\langle \theta_e^2 \rangle W_\phi \, d\phi$, where the electron polar scattering angle $\theta_e \simeq u\sqrt{z^{2/3}-1}/\gamma$ and $W_\phi$ is the instantaneous rate of photon emission per unit phase. In the limit $\chi_e \ll 1$, $\langle \theta_e^2 \rangle \simeq 13\chi_e^2/(30\gamma^2)$ and $W_\phi \simeq 5\alpha m \chi_e/(4\sqrt{3}\gamma\omega)$. Assuming that the temporal profile $g(\phi)$ is slowly varying, we find

$$\delta_e^2 = \delta_0^2 + \frac{26\sqrt{3}\alpha}{27\pi} \frac{a_0^3 \omega^2}{m^2} \int_{-\infty}^{\infty} g^3(\phi) \, d\phi, \tag{6}$$

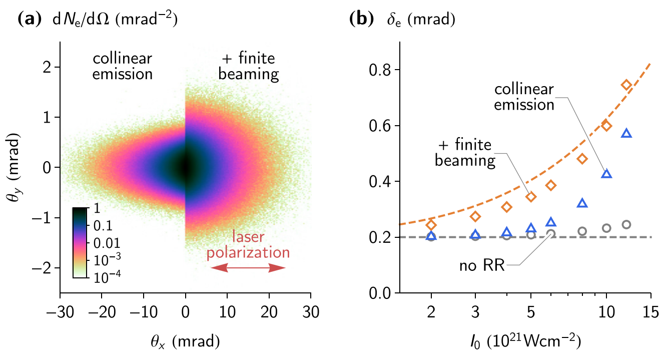


FIG. 5. Effect of the transverse recoil on the electron angular distribution, in the collision of a 500-MeV electron beam and a linearly polarized laser pulse with peak intensity $I_0$: (a) $\theta_x$-$\theta_y$ distribution at $I_0 = 5 \times 10^{21}$ W cm$^{-2}$; (b) rms $\theta_y$ from simulations (points), its initial value (gray, dashed), and that predicted by Eq. (6) (orange, dashed).

where $\delta_0$ is the initial divergence of the electron beam. If the intensity profile is a Gaussian with peak $I_0$ and FWHM duration $\tau$, $\int_{-\infty}^{\infty} g^3(\phi)\,d\phi = \omega\tau\sqrt{\pi/(6\ln 2)}$ and $\delta_e[\mathrm{mrad}] \simeq 0.086 I_0^{3/4}[10^{21}\ \mathrm{W\ cm^{-2}}]\tau^{1/2}[10\,\mathrm{fs}]$.

We now compare this prediction to the results of 3D simulations of laser-electron collisions. It is essential to account for multidimensional effects, because there is a ponderomotive contribution to the electron deflection [49], which is enhanced by energy losses to radiation emission. To mitigate this competing source of divergence increase, we consider collisions with frequency-doubled laser pulses that are focused to relatively large spot sizes. This exploits the fact that the ponderomotive force, and thus the divergence it induces, are proportional to the gradient of the squared vector potential, $\nabla a^2(x, y) \propto I_0\lambda^2\rho/w_0^2$, whereas the increase in divergence due to finite beaming $\delta_e \propto I_0^{3/4}$ depends only on intensity. The electron beam is initialized with mean energy 500 MeV, energy spread 100 MeV, divergence $\delta_0 = 0.2$ mrad, and size $\rho = 1.0\,\mu$m (all rms), which corresponds to $\epsilon_\perp = 0.2$ mm mrad [45,46]. The frequency-doubled laser pulse has wavelength $0.4\,\mu$m, has duration 15 fs, and is focused to a spot of size $w_0 = 5\,\mu$m and peak intensity $5 \times 10^{21}$ W cm$^{-2}$.

The electron angular distributions for this particular configuration are shown in Fig. 5(a); the variation of the rms angle with peak intensity (all other parameters unchanged) is shown in Fig. 5(b). We see that the transverse recoil leads to a greater increase in the perpendicular divergence than quantum radiation reaction alone (i.e., if emission and recoil are assumed to be collinear with the electron initial momentum). The rms perpendicular angle obtained in the simulations agrees well with Eq. (6). These results are unchanged if the simulations are rerun with a maximum permitted photon formation length of $L_f = \lambda/10$, using the procedure given in Sec. II. This confirms that the beaming of the radiation is important for photons that are sufficiently energetic to affect the electron, unlike interference effects [28]. The challenge in realizing such measurements is the high degree of control required over both electron beam and laser pulse. Furthermore, we cannot simply increase the peak intensity to yield a larger value of $\delta_e$, as Eq. (6) suggests, because this enhances radiative energy losses and thus the ponderomotive deflection that masks the relevant signal. We will explore such effects in detail elsewhere.

## V. CONCLUSIONS

The radiation emitted by ultrarelativistic charged particles is strongly beamed in the direction parallel to the particle velocity. Despite the smallness of the opening angle, we have shown that implementation of a photon emission rate that is resolved in scattering angle as well as energy is necessary for accurate simulations of radiation generation in the quantum regime. The finite beaming is particularly important for moderate-energy photons, which are emitted into a broader range of angles.

The finite emission angle means that there is a component of the recoil that is perpendicular to the unperturbed momentum. While negligible in many high-intensity scenarios of interest, we have shown that this transverse recoil leads to a lower bound on the divergence of the electron beam in the direction perpendicular to the plane defined by the unperturbed momentum and the force of the external electromagnetic field. The increase in the out-of-plane momentum is a purely quantum effect, even though radiation beaming is a feature of the classical theory as well. This is because the number of emissions $N_\gamma \to \infty$ in the limit $\hbar \to 0$, which averages the recoil over the arbitrary azimuthal angle. In the quantum regime, the number of emissions is finite and therefore the change in transverse momentum is not completely compensated. The consequent increase in the electron-beam divergence is a signature of radiation reaction dynamics that go beyond the stochastic effects previously considered [50–52].

Beyond the interaction with a single laser pulse examined here, it is possible that the transverse recoil affects cascade development in an EM standing wave [19–21], because it would displace electrons from electric-field antinodes [53], where the most energetic photons are emitted. It might also seed plasma instabilities in dipole-wave-driven cascades [54].

## ACKNOWLEDGMENTS

The authors acknowledge support from the Knut and Alice Wallenberg Foundation (T.G.B., M.M.), Laboratory Directed Research and Development funding from Lawrence Berkeley National Laboratory provided by the Director, and the U.S. Department of Energy Office of Science, Offices of High Energy Physics and Fusion Energy Sciences (through LaserNetUS), under Contract No. DE-AC02-05CH11231 (S.S.B.), the U.S. Army Research Office under Grant No. W911NF-16-1-0044 (D.S.), and the Swedish Research Council under Grants No. 2013-4248 and No. 2016-03329 (M.M.). Simulations were performed on resources provided by the Swedish National Infrastructure for Computing at the High Performance Computing Centre North.

[1] J. H. Sung, H. W. Lee, J. Y. Yoo, J. W. Yoon, C. W. Lee, J. M. Yang, Y. J. Son, Y. H. Jang, S. K. Lee, and C. H. Nam, 4.2 PW, 20 fs Ti:sapphire laser at 0.1 Hz, Opt. Lett. **42**, 2058 (2017).

[2] H. Kiriyama, A. S. Pirozhkov, M. Nishiuchi, Y. Fukuda, K. Ogura, A. Sagisaka, Y. Miyasaka, M. Mori, H. Sakaki, N. P. Dover, K. Kondo, J. K. Koga, T. Zh. Esirkepov, M. Kando, and K. Kondo, High-contrast high-intensity repetitive petawatt laser, Opt. Lett. **43**, 2595 (2018).

[3] K. Nakamura, H. Mao, A. J. Gonsalves, H. Vincenti, D. E. Mittelberger, J. Daniels, A. Magana, C. Toth, and W. P. Leemans, Diagnostics, control and performance parameters for the BELLA high repetition rate petawatt class laser, IEEE J. Quantum Electron. **53**, 1 (2017).

[4] S. Corde, E. Adli, J. M. Allen, W. An, C. I. Clarke, C. E. Clayton, J. P. Delahaye, J. Frederico, S. Gessner, S. Z. Green, M. J. Hogan, C. Joshi, N. Lipkowitz, M. Litos, W. Lu, K. A. Marsh, W. B. Mori, M. Schmeltz, N. Vafaei-Najafabadi, D. Walz, V. Yakimenko, and G. Yocky, Multi-gigaelectronvolt acceleration of positrons in a self-loaded plasma wakefield, Nature (London) **524**, 442 (2015).

[5] E. Adli, A. Ahuja, O. Apsimon, R. Apsimon, A.-M. Bachmann, D. Barrientos, F. Batsch, J. Bauche, V. K. Berglyd Olsen, M. Bernardini *et al.* (AWAKE Collaboration), Acceleration of electrons in the plasma wakefield of a proton bunch, Nature (London) **561**, 363 (2018).

[6] A. J. Gonsalves, K. Nakamura, J. Daniels, C. Benedetti, C. Pieronek, T. C. H. de Raadt, S. Steinke, J. H. Bin, S. S. Bulanov, J. van Tilborg, C. G. R. Geddes, C. B. Schroeder, C. Tóth, E. Esarey, K. Swanson, L. Fan-Chiang, G. Bagdasarov, N. Bobrova, V. Gasilov, G. Korn, P. Sasorov, and W. P. Leemans, Petawatt Laser Guiding and Electron Beam Acceleration to 8 GeV in a Laser-Heated Capillary Discharge Waveguide, Phys. Rev. Lett. **122**, 084801 (2019).

[7] J. M. Cole, K. T. Behm, E. Gerstmayr, T. G. Blackburn, J. C. Wood, C. D. Baird, M. J. Duff, C. Harvey, A. Ilderton, A. S. Joglekar, K. Krushelnick, S. Kuschel, M. Marklund, P. McKenna, C. D. Murphy, K. Poder, C. P. Ridgers, G. M. Samarin, G. Sarri, D. R. Symes, A. G. R. Thomas, J. Warwick, M. Zepf, Z. Najmudin, and S. P. D. Mangles, Experimental Evidence of Radiation Reaction in the Collision of a High-Intensity Laser Pulse with a Laser-Wakefield Accelerated Electron Beam, Phys. Rev. X **8**, 011020 (2018).

[8] K. Poder, M. Tamburini, G. Sarri, A. Di Piazza, S. Kuschel, C. D. Baird, K. Behm, S. Bohlen, J. M. Cole, D. J. Corvan, M. Duff, E. Gerstmayr, C. H. Keitel, K. Krushelnick, S. P. D. Mangles, P. McKenna, C. D. Murphy, Z. Najmudin, C. P. Ridgers, G. M. Samarin, D. R. Symes, A. G. R. Thomas, J. Warwick, and M. Zepf, Experimental Signatures of the Quantum Nature of Radiation Reaction in the Field of an Ultraintense Laser, Phys. Rev. X **8**, 031004 (2018).

[9] C. Bula, K. T. McDonald, E. J. Prebys, C. Bamber, S. Boege, T. Kotseroglou, A. C. Melissinos, D. D. Meyerhofer, W. Ragg, D. L. Burke, R. C. Field, G. Horton-Smith, A. C. Odian, J. E. Spencer, D. Walz, S. C. Berridge, W. M. Bugg, K. Shmakov, and A. W. Weidemann, Observation of Nonlinear Effects in Compton Scattering, Phys. Rev. Lett. **76**, 3116 (1996).

[10] D. L. Burke, R. C. Field, G. Horton-Smith, J. E. Spencer, D. Walz, S. C. Berridge, W. M. Bugg, K. Shmakov, A. W. Weidemann, C. Bula, K. T. McDonald, E. J. Prebys, C. Bamber, S. J. Boege, T. Koffas, T. Kotseroglou, A. C. Melissinos, D. D. Meyerhofer, D. A. Reis, and W. Ragg, Positron Production in Multiphoton Light-by-Light Scattering, Phys. Rev. Lett. **79**, 1626 (1997).

[11] Gerard A. Mourou, T. Tajima, and Sergei V. Bulanov, Optics in the relativistic regime, Rev. Mod. Phys. **78**, 309 (2006).

[12] M. Marklund and Padma K. Shukla, Nonlinear collective effects in photon-photon and photon-plasma interactions, Rev. Mod. Phys. **78**, 591 (2006).

[13] A. Di Piazza, C. Müller, K. Z. Hatsagortsyan, and C. H. Keitel, Extremely high-intensity laser interactions with fundamental quantum systems, Rev. Mod. Phys. **84**, 1177 (2012).

[14] V. I. Ritus, Quantum effects of the interaction of elementary particles with an intense electromagnetic field, J. Sov. Laser Res. **6**, 497 (1985).

[15] A. K. Harding and D. Lai, Physics of strongly magnetized neutron stars, Rep. Prog. Phys. **69**, 2631 (2006).

[16] C. P. Ridgers, C. S. Brady, R. Duclous, J. G. Kirk, K. Bennett, T. D. Arber, A. P. L. Robinson, and A. R. Bell, Dense Electron-Positron Plasmas and Ultraintense $\gamma$ Rays from Laser-Irradiated Solids, Phys. Rev. Lett. **108**, 165006 (2012).

[17] T. Nakamura, J. K. Koga, T. Zh. Esirkepov, M. Kando, G. Korn, and S. V. Bulanov, High-Power $\gamma$-Ray Flash Generation in Ultraintense Laser-Plasma Interactions, Phys. Rev. Lett. **108**, 195001 (2012).

[18] D. J. Stark, T. Toncian, and A. V. Arefiev, Enhanced Multi-MeV Photon Emission by a Laser-Driven Electron Beam in a Self-Generated Magnetic Field, Phys. Rev. Lett. **116**, 185003 (2016).

[19] A. R. Bell and J. G. Kirk, Possibility of Prolific Pair Production with High-Power Lasers, Phys. Rev. Lett. **101**, 200403 (2008).

[20] A. M. Fedotov, N. B. Narozhny, G. Mourou, and G. Korn, Limitations on the Attainable Intensity of High Power Lasers, Phys. Rev. Lett. **105**, 080402 (2010).

[21] S. S. Bulanov, T. Zh. Esirkepov, A. G. R. Thomas, J. K. Koga, and S. V. Bulanov, Schwinger Limit Attainability with Extreme Power Lasers, Phys. Rev. Lett. **105**, 220407 (2010).

[22] E. N. Nerush, I. Yu. Kostyukov, A. M. Fedotov, N. B. Narozhny, N. V. Elkina, and H. Ruhl, Laser Field Absorption in Self-Generated Electron-Positron Pair Plasma, Phys. Rev. Lett. **106**, 035001 (2011).

[23] D. N. Papadopoulos, J. P. Zou, C. Le Blanc, G. Chériaux, P. Georges, F. Druon, G. Mennerat, P. Ramirez, L. Martin, A. Fréneaux, A. Beluze, N. Lebas, P. Monot, F. Mathieu, and P. Audebert, The Apollon 10 PW laser: experimental and theoretical investigation of the temporal characteristics, High Power Laser Science and Engineering **4**, e34 (2016).

[24] S. Weber, S. Bechet, S. Borneis, L. Brabec, M. Bučka, E. Chacon-Golcher, M. Ciappina, M. DeMarco, A. Fajstavr, K. Falk, E.-R. Garcia, J. Grosz, Y.-J. Gu, J.-C. Hernandez, M. Holec, P. Janečka, M. Jantač, M. Jirka, H. Kadlecova, D. Khikhlukha, O. Klimo, G. Korn, D. Kramer, D. Kumar, T. Lastovička, P. Lutoslawski, L. Morejon, V. Olšovcová, M. Rajdl, O. Renner, B. Rus, S. Singh, M. Šmid, M. Sokol, R. Versaci, R. Vrána, M. Vranic, J. Vyskočil, A. Wolf, and Q. Yu, P3: An installation for high-energy density plasma physics and ultra-high intensity laser-matter interaction at ELI-Beamlines, Matter Radiation at Extremes **2**, 149 (2017).

[25] S. Gales, K. A. Tanaka, D. L. Balabanski, F. Negoita, D. Stutman, O. Tesileanu, C. A. Ur, D. Ursescu, I. Andrei,

S. Ataman, M. O. Cernaianu, L. D'Alessi, I. Dancus, B. Diaconescu, N. Djourelov, D. F. Filipescu, P. Ghenuche, D. G. Ghita, C. Matei, K. Seto, M. Zeng, and N. V. Zamfir, The extreme light infrastructure–nuclear physics (ELI-NP) facility: new horizons in physics with 10 PW ultra-intense lasers and 20 MeV brilliant gamma beams, Rep. Prog. Phys. **81**, 094301 (2018).

[26] C. P. Ridgers, J. G. Kirk, R. Duclous, T. G. Blackburn, C. S. Brady, K. Bennett, T. D. Arber, and A. R. Bell, Modelling gamma-ray photon emission and pair production in high-intensity laser-matter interactions, J. Comput. Phys. **260**, 273 (2014).

[27] A. Gonoskov, S. Bastrakov, E. Efimenko, A. Ilderton, M. Marklund, I. Meyerov, A. Muraviev, A. Sergeev, I. Surmin, and E. Wallin, Extended particle-in-cell schemes for physics in ultrastrong laser fields: Review and developments, Phys. Rev. E **92**, 023305 (2015).

[28] T. G. Blackburn, D. Seipt, S. S. Bulanov, and M. Marklund, Benchmarking semiclassical approaches to strong-field QED: Nonlinear Compton scattering in intense laser pulses, Phys. Plasmas **25**, 083108 (2018).

[29] V. N. Baier, V. M. Katkov, and V. M. Strakhovenko, *Electromagnetic Processes at High Energies in Oriented Single Crystals* (World Scientific, Singapore, 1998).

[30] F. Sauter, Uber das Verhalten eines Elektrons im homogenen elektrischen Feld nach der relativistischen Theorie Diracs, Z. Phys. **69**, 742 (1931).

[31] J. Schwinger, On gauge invariance and vacuum polarization, Phys. Rev. **82**, 664 (1951).

[32] D. Seipt, T. Heinzl, M. Marklund, and S. S. Bulanov, Depletion of Intense Fields, Phys. Rev. Lett. **118**, 154803 (2017).

[33] V. Dinu, C. Harvey, A. Ilderton, M. Marklund, and G. Torgrimsson, Quantum Radiation Reaction: From Interference to Incoherence, Phys. Rev. Lett. **116**, 044801 (2016).

[34] W. H. Furry, On bound states and scattering in positron theory, Phys. Rev. **81**, 115 (1951).

[35] D. Seipt and B. Kämpfer, Nonlinear Compton scattering of ultrashort intense laser pulses, Phys. Rev. A **83**, 022101 (2011).

[36] D. Seipt, V. Kharin, S. Rykovanov, A. Surzhykov, and S. Fritzsche, Analytical results for nonlinear Compton scattering in short intense laser pulses, J. Plasma Phys. **82**, 655820203 (2016).

[37] A. Di Piazza, K. Z. Hatsagortsyan, and C. H. Keitel, Quantum Radiation Reaction Effects in Multiphoton Compton Scattering, Phys. Rev. Lett. **105**, 220403 (2010).

[38] C. N. Harvey, A. Ilderton, and B. King, Testing numerical implementations of strong-field electrodynamics, Phys. Rev. A **91**, 013822 (2015).

[39] A. Ilderton, B. King, and D. Seipt, Extended locally constant field approximation for nonlinear Compton scattering, Phys. Rev. A **99**, 042121 (2019).

[40] D. Seipt and A. G. R. Thomas, A Frenet-Serret interpretation of particle dynamics in high-intensity laser fields, Plasma Phys. Control. Fusion **61**, 074005 (2019).

[41] A. Di Piazza, M. Tamburini, S. Meuren, and C. H. Keitel, Implementing nonlinear Compton scattering beyond the local-constant-field approximation, Phys. Rev. A **98**, 012134 (2018).

[42] A. Di Piazza, M. Tamburini, S. Meuren, and C. H. Keitel, Improved local-constant-field approximation for strong-field QED codes, Phys. Rev. A **99**, 022125 (2019).

[43] B. King, A uniform locally constant field approximation for photon-seeded pair production, arXiv:1908.06985 (2019).

[44] L. D. Landau and E. M. Lifshitz, *The Classical Theory of Fields*, The Course of Theoretical Physics Vol. 2 (Butterworth-Heinemann, Oxford, 1987).

[45] G. R. Plateau, C. G. R. Geddes, D. B. Thorn, M. Chen, C. Benedetti, E. Esarey, A. J. Gonsalves, N. H. Matlis, K. Nakamura, C. B. Schroeder, S. Shiraishi, T. Sokollik, J. van Tilborg, C. Toth, S. Trotsenko, T. S. Kim, M. Battaglia, Th. Stöhlker, and W. P. Leemans, Low-Emittance Electron Bunches from a Laser-Plasma Accelerator Measured using Single-Shot X-Ray spectroscopy, Phys. Rev. Lett. **109**, 064802 (2012).

[46] R. Weingartner, S. Raith, A. Popp, S. Chou, J. Wenz, K. Khrennikov, M. Heigoldt, A. R. Maier, N. Kajumba, M. Fuchs, B. Zeitler, F. Krausz, S. Karsch, and F. Grüner, Ultralow emittance electron beams from a laser-wakefield accelerator, Phys. Rev. ST Accel. Beams **15**, 111302 (2012).

[47] Y. I. Salamin, Fields of a Gaussian beam beyond the paraxial approximation, Appl. Phys. B **86**, 319 (2007).

[48] T. O. Raubenheimer, The generation and acceleration of low emittance flat beams for future linear colliders, Technical Report No. SLAC-R-387, 1991 (unpublished).

[49] B. Quesnel and P. Mora, Theory and simulation of the interaction of ultraintense laser pulses with electrons in vacuum, Phys. Rev. E **58**, 3719 (1998).

[50] D. G. Green and C. N. Harvey, Transverse Spreading of Electrons in High-Intensity Laser Fields, Phys. Rev. Lett. **112**, 164801 (2014).

[51] M. Vranic, T. Grismayer, R. A. Fonseca, and L. O. Silva, Quantum radiation reaction in head-on laser-electron beam interaction, New J. Phys. **18**, 073035 (2016).

[52] Y.-F. Li, Y.-T. Zhao, K. Z. Hatsagortsyan, C. H. Keitel, and J.-X. Li, Electron-angular-distribution reshaping in the quantum radiation-dominated regime, Phys. Rev. A **98**, 052120 (2018).

[53] B. King and H. Hu, Classical and quantum dynamics of a charged scalar particle in a background of two counterpropagating plane waves, Phys. Rev. D **94**, 125010 (2016).

[54] E. S. Efimenko, A. V. Bashinov, S. I. Bastrakov, A. A. Gonoskov, A. A. Muraviev, I. B. Meyerov, A. V. Kim, and A. M. Sergeev, Extreme plasma states in laser-governed vacuum breakdown, Sci. Rep. **8**, 2329 (2018).